A Robot-Eye Control System Based on Binocular Motor Mechanism

Xiaolin Zhang and Hidetoshi Wakamatsu, *Member*

***Abstract* — A robot-eye system with a similar control system to the synthesized binocular motor system model based on physiological and anatomical fact is built. The robot-eye system shows some special characteristics that exist in human-eye movements but have not been realized in conventional robot eyes. The main characteristics of the robot-eye system are:**

(1) The both eyes will not gaze at two different targets at the same time, i.e. the both eyes move in tandem and have the same target in the central pits. This characteristic is considered a basic condition for structuring stereo-image using the image signals from both eyes.

(2) If one eye is shut or obstructed by an obstacle, the eye will follow up the movement of the other eye so that it can find the target swiftly when the eye is opened or the obstacle is removed.

(3) The binocular motor system can realize VOR not only for head rotation, but also for head translations in order to compensate for the blurs caused by head movements. (250 words)

***Index Terms*-- binocular motor system model, robot, conjugate eye movement, vergence eye movement, VOR.**

I. Introduction

Unlike chameleon eyes, human eyes cannot gaze at two different targets at one time. Instead, a human's eyes can easily catch the same point of the subject at both central pits and use the two symmetrical images from both retinas to produce a stereovision space in the visual cortex. In this paper, the point viewed is called a target. We call the ability to gaze at the same target by both eyes simultaneously as "same point gazing tendency," and we believe it to be one of the basic conditions for structuring a stereovision in the visual cortex. The proposed robot-eye system, consisting of the same control system as the binocular motor model described in the last paper [17], will demonstrate such a characteristic.

Human eyes always show conjugate movement, even when one eye is shut or blocked by an obstacle. An obvious function of the characteristic is that when the eye is opened or the obstacle is taken off, the eye will follow up the target pursued by the other eye quickly. The conjugate eye movements are realized using the proposed robot-eye system. Because the eyes of the robot-eye system are not fixed to each other like conventional robot eyes [1]-[3], they also could perform vergence eye movement simultaneously.

To obtain 3-D information about an object, active visual sensors have been used in conventional researches, with good results [5]-[12]. However, the most active visual sensors use independent systems to control each eye. So these visual sensor systems can not realize the human characteristics outlined above.

To fix the optical lines on the target on the head movement, the vestibulo-ocular reflex (VOR) plays an important role in the ocular motor system. Wagner R, Galiana H and others had proposed binocular motor robots, which realized VOR for head rotations [13], [14]. In the last paper, we proposed a binocular motor system model that included VOR mechanisms not only for head rotation (VOR-R) but also for head translation (VOR-T, conventionally named as the otolith-ocular reflex [4]). In this paper, we use our robot-eye system to realize all types of VOR in horizontal eye movement.

II. Structure of the Robot-Eyes System

In this research, we constructed a binocular motor control device (robot eyes) with the same system structure as the binocular motor system model that we had proposed on the basis of the anatomic structure and physiological function of the brainstem [17], as shown in Fig.1.

This robot has 2 degrees of freedom for each "eyeball" and 1 degree of freedom for the neck. DC motors are used as the actuators (Maxson DC motor, 2322-982-52-235-200 for eyeballs, and M99051-A-1 for neck, Swiss made). The image signals from cameras (CCD camera, TOSHIBA IK-CU43) are taken into the computer via an image processing board (MATROX METEOR II). The target's position and velocity related to the optical line (camera's central line) can be obtained by image processing using the computer. The results of the image processing are transferred in real time through a PIO board to the computer used for robot control. The rotary angle of each motor can be detected using its own encoder (MTL, MEH-20-2000, Japan). The encoder in the neck motor will be substituted for the horizontal semicircular canals. Figure 2 is the exterior of the robot-eye system.

Figure 3(a) is the layout of the robot eyes. Figure 3(b) is the coordinate system of the robot eyes. In Figure 3(b), $O_{E\text{-}l}$ and $O_{E\text{-}r}$ are the origins of coordinate systems for both cameras ($x_{E\text{-}l}$-$y_{E\text{-}l}$-$z_{E\text{-}l}$, and $x_{E\text{-}r}$-$y_{E\text{-}r}$-$z_{E\text{-}r}$, we called them as eyeball fixed coordinate system). $O_{E\text{-}l}$ is defined at the crossing point of motor 1 and motor 3, $x_{E\text{-}l}$-axis is defined on the central line of left camera, and $y_{E\text{-}l}$-axis is defined on parallel with lateral pixels line of the CCD camera. The right camera fixed coordinate system $x_{E\text{-}r}$-$y_{E\text{-}r}$-$z_{E\text{-}r}$ is similar to the left one. The left orbit fixed coordinates systems ($x_{O\text{-}l}$-$y_{O\text{-}l}$-$z_{O\text{-}l}$) is defined as in Fig. 3(b), where $y_{O\text{-}l}$-axis is defined on the axis of motor 3, and $z_{E\text{-}l}$-axis is defined on the axis of motor 1. The right orbit fixed coordinates systems ($x_{O\text{-}r}$-$y_{O\text{-}r}$-$z_{O\text{-}r}$) is similar to the left.

This study was presented in part in proceedings of the 15th symposium on Biological and Physiological Engineering, sponsored by SICE, Japan, in 2000.

The authors are with the Faculty of Medicine, Tokyo Medical and Dental University.

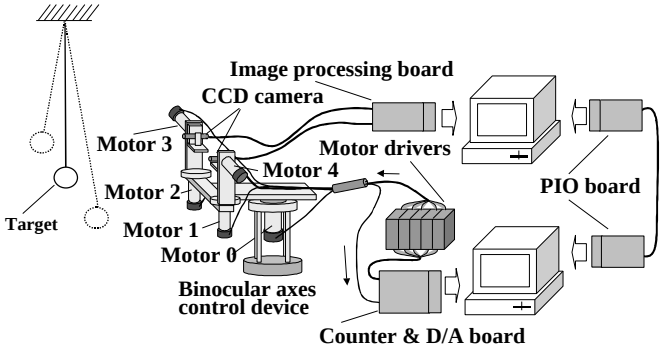

Fig. 1 Structure of robot eyes according to binocular motor system model

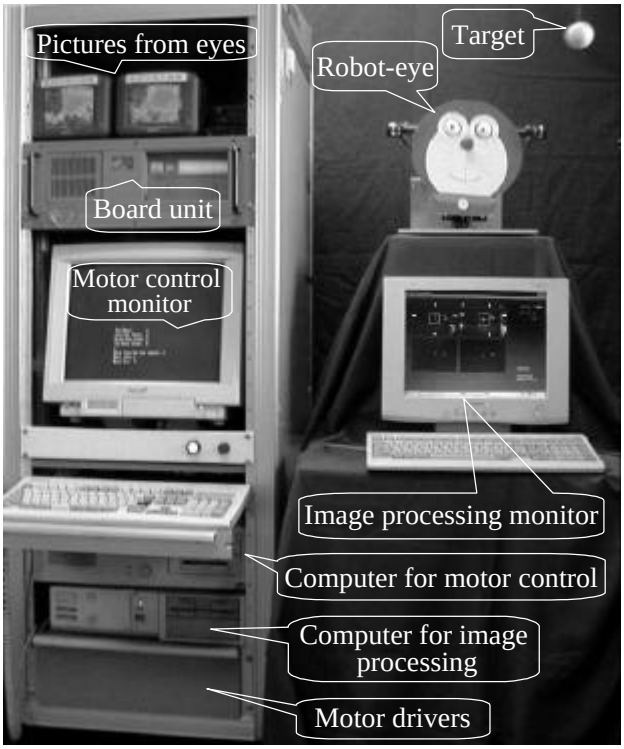

Fig.2 Entire exterior of robot-eyes system

O_H is the origin of the head-fixed coordinates system (x_H-y_H-z_H) which is defined at the point of the axes of motor 0 crossed to the horizontal plane through $O_{E\text{-}l}$ and $O_{E\text{-}r}$. O_B is the origin of the base coordinates system (x_B-y_B-z_B).

Since we consider only horizontal eye movements, the control loops of motor 3 and 4 will not be explained here, i.e. the translation of the head in z_H axis direction and q_3, q_4 will not be considered. So, the horizontal coordinate systems of Fig. 3(a) are drawn in Fig. 4. Since the robot-eye system has no degree for translation, in the real system $x_h = 0$, $y_h = 0$. In the experiments of the case of head translation, $x_h(t)$, $y_h(t)$ and "retinal slip" ($j_{D\text{-}l}$, $j_{D\text{-}r}$), will be given by computer directly. From Fig. 4, the desired values of each eyeball are given as the following equations:

$$j_l(t) = q_0(t) - \tan^{-1}\frac{y_t(t) - y_h(t) - r_{he}\sin(q_0(t) + j_{he})}{x_t(t) - x_h(t) - r_{he}\cos(q_0(t) + j_{he})} \quad (1)$$

$$j_r(t) = q_0(t) - \tan^{-1}\frac{y_t(t) - y_h(t) - r_{he}\sin(q_0(t) - j_{he})}{x_t(t) - x_h(t) - r_{he}\cos(q_0(t) - j_{he})} \quad (2)$$

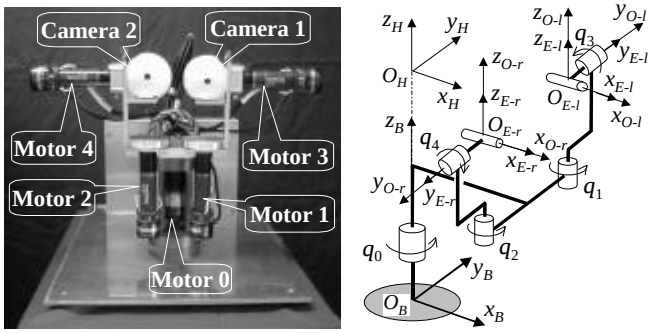

(a) Robot-eyes layout

(b) Coordinate frames

Fig. 3 Structure of robot eyes

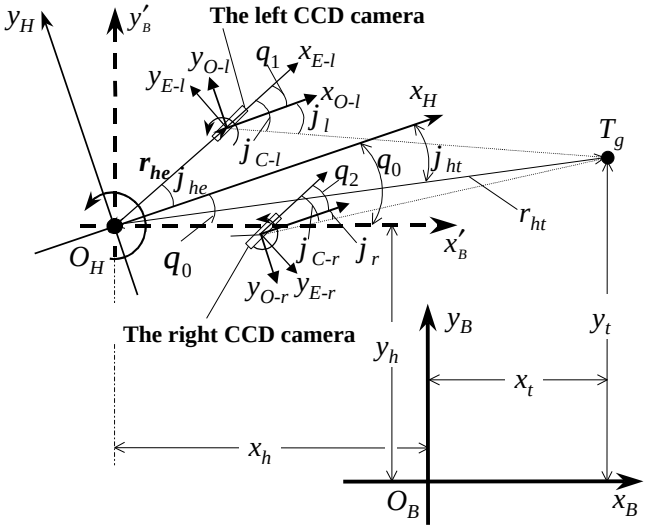

Fig. 4 Horizontal coordinate systems for robot-eye systems

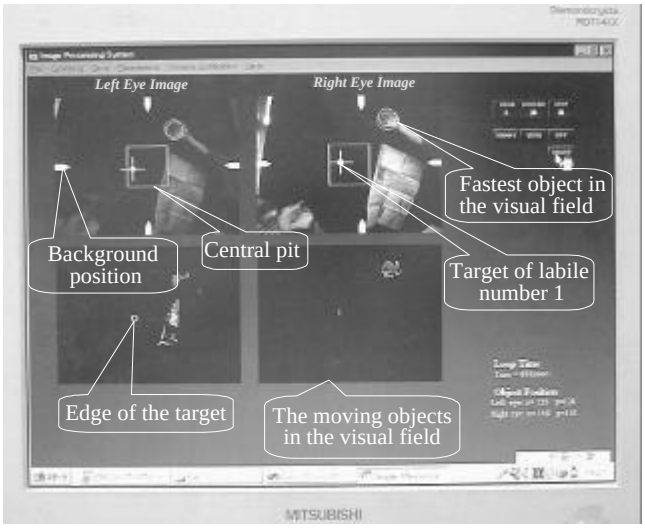

Fig.5 The results of image processing

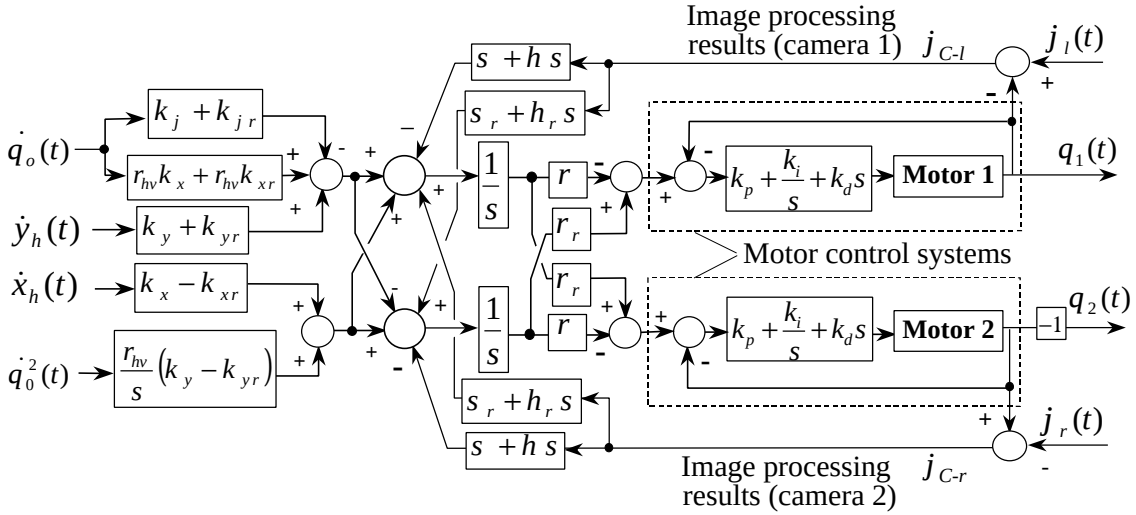

Fig. 6 Block diagram for robot-eye control system [17]

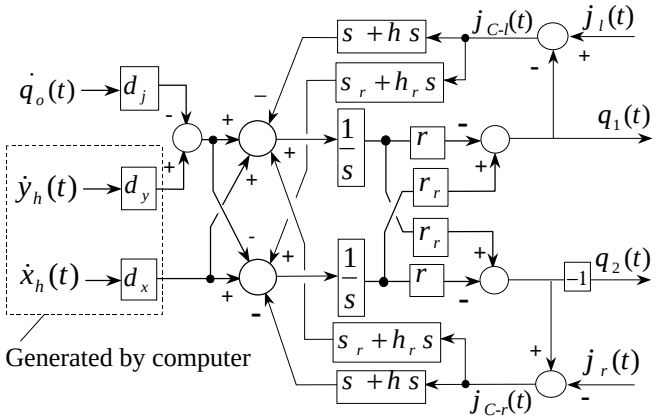

Fig.7 Simplified block diagram of robot-eye system

III. IMAGE PROCESSING FOR THE ROBOT EYES

For this paper, we used a white ball as the target of the robot-eye system. Image processing includes: 1) obtaining the gray-level histogram, 2) binalization using the histogram, 3) edge extraction, 4) circles detection using Hough transformation, 5) checking the color of original image in the circles, 6) labeling the extracted circles, 7) calculating the velocity of the circles, 8) detecting the background movement, 9) detecting the moving object related with background. Figure 5 shows an example of the display of the computer for image processing. The mark + is the position of the target which labile number is 1, obtained through the previous methods 1)-7). The mark ○ represents the object that is moving fastest in the visual field. The arrows at each side of the visual fields represent the position of the background. It is not the main object to introduce the image processing in detail here. In the following experiments, only the target's position and its velocity are used. The processing cycle time is about 66-166 ms.

IV THE CONTROL SYSTEM FOR THE ROBOT EYES

The binocular motor model we had proposed on the basis of the anatomic structure and physiological function of the brainstem is shown in Figure 6 [17]. The motor control systems (in the dashed-line boxes) are based on the PID control law, and the parameters of PID control are defined by the ultimate sensitivity method. The sampling time is 3ms. As the motor control systems are accurate enough compared with the image detecting errors and delays, in this paper, we may to consider the transfer functions of motor control systems as 1. Set k_y=k_{yr}, the influence of centrifugal force will be canceled, and unify the parameters as,

$$d_j = k_j + k_{jr} - r_{ve}k_x - r_{ve}k_{xr}$$
$$d_x = k_x - k_{xr},\ d_y = k_y + k_{yr}$$

Figure 6 can be simplified as Fig.7.

From Fig.7 the following equation is obtained.

$$\begin{bmatrix} q_1(s) \\ q_2(s) \end{bmatrix} = -\frac{d_x}{s - s_r + \left(\frac{1}{r - r_r} + h - h_r\right)s} \begin{bmatrix} \dot{x}_h(s) \\ -\dot{x}_h(s) \end{bmatrix}$$
$$+\frac{1}{2}\frac{s - s_r + hs - h_r s}{s - s_r + \left(\frac{1}{r - r_r} + h - h_r\right)s} \begin{bmatrix} j_l(s) - j_r(s) \\ j_r(s) - j_l(s) \end{bmatrix}$$
$$-\frac{1}{s + s_r + \left(\frac{1}{r + r_r} + h + h_r\right)s} \begin{bmatrix} d_y & d_j \\ d_y & d_j \end{bmatrix} \begin{bmatrix} \dot{y}_h(s) \\ \dot{q}_0(s) \end{bmatrix}$$
$$+\frac{1}{2}\frac{s + s_r + hs + h_r s}{s + s_r + \left(\frac{1}{r + r_r} + h + h_r\right)s} \begin{bmatrix} j_l(s) + j_r(s) \\ j_r(s) + j_l(s) \end{bmatrix} \quad (3)$$

Since the robot-eye system has only one encoder to detect the rotational angle of head q_0, and no sensor is designed to detect the head translation x_h and y_h, in this paper the input signals $\dot{x}_h$ and $\dot{y}_h$ are generated by the computer directly.

From (3), a sufficient condition can be obtained as the following equation [17]:

$$r > r_r,\quad s > s_r,\quad h > h_r,\quad d_x > 0,\quad d_y > 0 \quad (4)$$

Here set

$$d_j = \frac{1}{r + r_r} \quad (5)$$

Since when (5) is stand the VOR-R will show the best performance [17].

According to equation (4) and (5), here defined that d_j=0.5, r = 1.5, r_r = 0.5, d_x=0.1 rad./m, σ = 1, σ_r =0.5, h = 0.5, h_r=0.2, d_y = 1.2 rad./m. All those parameters were selected by the experiments repetitively.

In the initial state, the x_H and y_H axis of the head fixed coordinate system of the robot-eye system are set to accord the base coordinate system, and the x_E and y_E axis of the eyeball fixed coordinate systems are set to accord the orbit fixed coordinate systems, i.e.

$$x_h(t) = 0 \text{ m}, \quad y_h(t) = 0 \text{ m},$$
$$q_0(t) = 0 \text{ rad}, \quad q_1(t) = 0 \text{ rad}, \quad q_2(t) = 0 \text{ rad}.$$

The target position is set at $x_t(0)$ =1 m, $y_t(0)$ = 0 m.

V Experiments to Confirm Characteristics of Conjugate and Vergence Eye Movement

A. The characteristics of same point gazing tendency

The faculty of conjugate eye movement means that two eyes cannot look at different targets at the same time. The skillful relation of conjugate and vergence movement of human eyes cause the abilities, such as that both eyes can easily catch the same target on the central pits of the retinas. In this experiment, we will confirm the occurrence of the same point gazing tendency in the robot eyes.

The circumstances of the experiments are shown in Fig. 8, and the movies can be downloaded from our homepage [18]. First, fix the head, set a fixed target in front of the head, then show a pendulum swinging from right to left. The weight on the top of the pendulum with the same shape as the first target becomes the second target. The experiment was repeated countless times. Each time, both eyes simultaneously looked at only one target, either the first or the second. One of the experiment results is shown in Fig. 9, which shows the moment that both eyes moved their gaze from the first to the second target.

For easy explanation, in Fig. 9 draw the desired values j_l and j_r calculated geometrically. Where ${}^1j_l$ and ${}^1j_r$ in Fig.9 are the locus of the first target related to each eyeball, ${}^2j_l$ and ${}^2j_r$ are the locus of the second target, and $j_{C\text{-}l}(t)$ and $j_{C\text{-}r}(t)$ are the "retinal slips" (errors detected by image processing). The t_1 shown in Fig. 9 is the instant that shows the second target to the robot eyes. The t_2 is the instant that the left eye recognizes the second target, and from t_3 to t_5, the left eye loses its target. t_4 and t_5 are the instants that the right eye and the left eye recognize the second target. Fig. 9 shows when the left eye recognizes the second target at t_2, the left eyeball (q_1) begins to leave the first target and pulls the right eyeball (q_2) to leave the first target too. This causes the right eye to recognize the second target (the object near the central pit will be processed in priority). There are cases when the right eye does not recognize the second target and pulls the left eyeball to recognize the first target again. Nevertheless, the optical lines of the eyeballs separate slowly and for only an instant when the two eyes recognize different targets, and they will tend to move together soon.

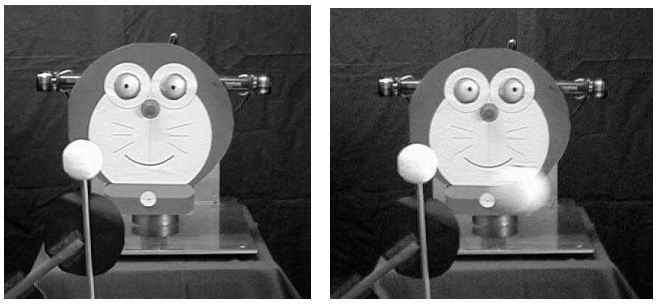

(a) Showing a first target (b) Showing the second target

Fig. 8 Circumstances of the experiments of same point gazing tendency [18].

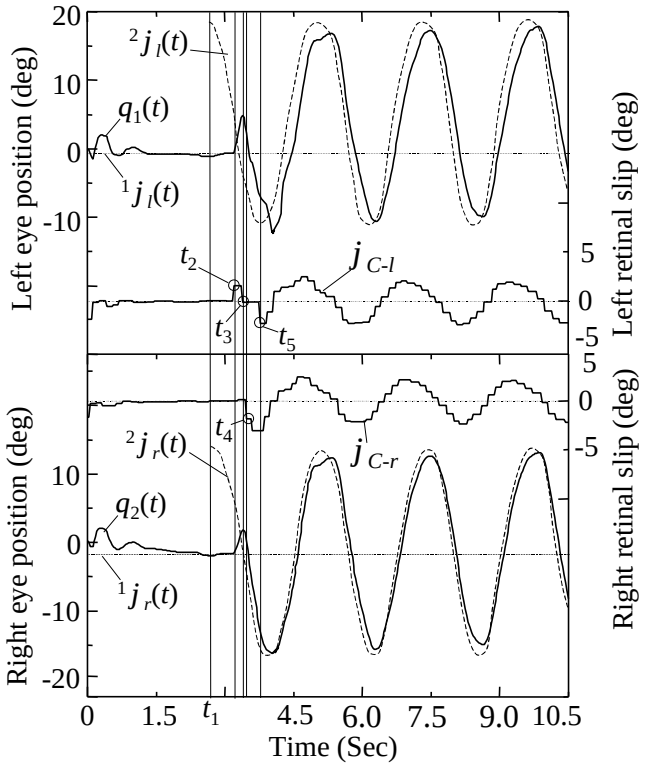

Fig. 9 The characteristic of eye movement by which two eyes gaze at only one target at the same time.

B. The characteristic when one eye is prevented from viewing the target

When an eye is shut or the target is blocked with an obstacle, the eye will move with the other eyeball. This characteristic lets the eye follow up to the target quickly when the obstacle is removed. The following experiment confirms the occurrence of conjugate eye movement:

Fix the head and set a target on the top of a pendulum, then swing it from right to left in front of the head. The circumstances of the experiments are shown in Fig. 10. One of the experiment results is shown in Fig. 11. In the term of t_1 to t_2, the left eye is intercepted using a mask as shown in Fig. 10 (a). Figure 11 shows that even though the left eye cannot follow the target accurately while it is blocked, it follows up the target very smoothly when the mask is taken off.

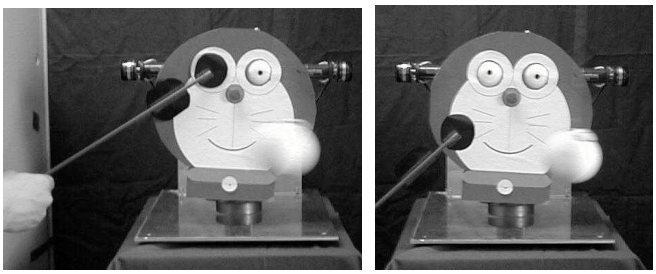

(a) Shutting the left eye (b) Taking off the obstacle

Fig. 10 The circumstances of the experiments of obstructing one eye's view for a moment [18].

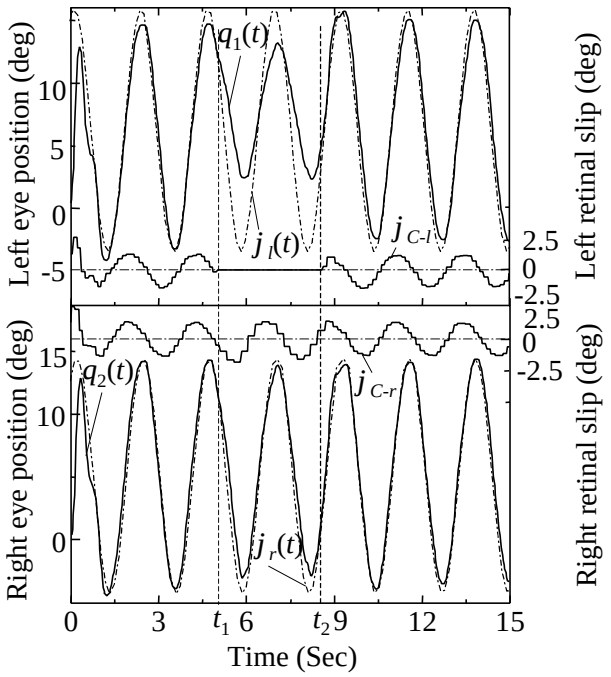

Fig. 11 Tracking of optic axes for smooth pursuit when the left "eye" was shut out in a term (t_1 to t_2).

C. Characteristics of vergence eye movement

If a binocular motor control system had only conjugate eye movements, the system would not have any significance because it would mean the two eyeballs were fixed to each other. Vergence eye movement is needed for catching a target at the central pits of both eyes when the target is approaching or receding from the eyes as shown in Fig. 12. To observe the characteristics of vergence eye movement of the robot eyes, the step response is obtained in the following experiment:

Fix the head and set the initial positions of each eyeball to parallel with the midline, namely,

$$x_h(t)=0 \text{ m}, y_h(t)=0 \text{ m},$$

$$q_0(t)=0 \text{ rad}, q_1(0)=0 \text{ rad}, q_2(0)=0 \text{ rad},$$

Setting a target at the position of

$$r_{ht}=0.2 \text{ m}, \; j_{ht} = -5 \text{ deg} = -0.087 \text{ rad}.$$

From (1) and (2), the desired values of each eyeball are given as the equations (7) and (8).

$$j_l(t) = j_{ot-l}(t) = -\tan^{-1}\frac{r_{ht}\sin j_{ht} - r_{he}\sin j_{he}}{r_{ht}\cos j_{ht} - r_{he}\cos j_{he}} \quad (7)$$

$$j_r(t) = -j_{ot-r}(t) = -\tan^{-1}\frac{r_{ht}\sin j_{ht} + r_{he}\sin j_{he}}{r_{ht}\cos j_{ht} - r_{he}\cos j_{he}} \quad (8)$$

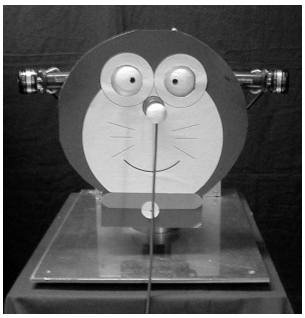

Fig. 12 The circumstances of the experiment of vergence [18].

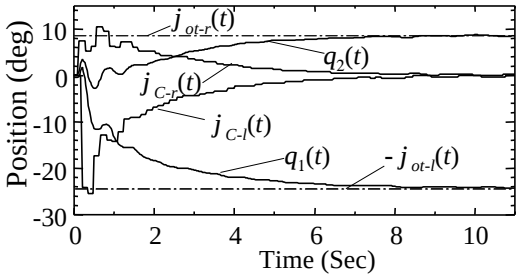

Fig. 13 Tracking of optic axes for vergence eye movement

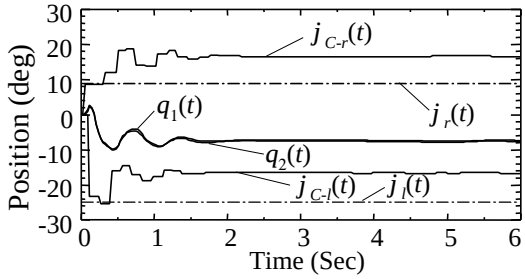

Fig. 14 Tracking of optic axes for optokinetic response when $r_1 = r_2$.

Since the robot eyes were designed as

$$r_{he}=0.09 \text{ m}, \; j_{he}=22.88 \text{ deg} = 0.400 \text{ rad}.$$

From equation (7), (8),

$$j_l = -24.3 \text{ deg} = -0.424 \text{ rad}, \; j_r=8.6 \text{ deg} = 0.150 \text{ rad}$$

are obtain. The experiment situation is shown in Fig. 13. Figure 13 shows the controlled errors ($j_{C-l}(t)$ and $j_{C-r}(t)$) became 0, and the eyeballs' positions ($q_1(t)$, $q_2(t)$) closed to the desired values (j_l, j_r). Figure 13 also shows that the settling times of vergence eye movement are much slower compared to those of conjugate eye movement.

From (3) if set $r = r_r$ or $s = s_r$, $h = h_r$, the vergence eye movement will disappear. The experiment of $r = r_r$ is shown in Fig. 14. Figure 14 shows $q_1(t)$ and $q_2(t)$ are moving together completely, i.e. there is no vergence movement.

VI The Experiments of VOR for Head Rotations

a) Fix the target and rotate the head according to the following equation:

$$q_0(t) = \frac{p}{6}\sin(\frac{p}{3}t) \quad (9)$$

In this case,

$$x_h(t) = y_h(t) = y_t(t) = 0 \text{ m}, \; x_t(t) = 1 \text{ m} \quad (10)$$

Figure 15(a) shows the result of the experiment. Since the left eye has the same characteristics as the right one, we show only the right eye's rotation $q_2(t)$ in Fig. 15. The desired value j_r in the figure is obtained from equation (8)

b) Cut the VOR control loop by setting

$$d_j = d_x = d_y = 0,$$

and do the same experiment as (a). The rotation of the right eyeball is shown in Fig. 15(b). Since there are not vestibular reflex control loops in the control systems, this experiment is similar to fixing the head and rotating the target around the head according to

$$j_{ht}(t) = -\frac{p}{6}\sin(\frac{p}{3}t) \tag{11}$$

c) Rotate the head according to equation (9) in darkness. In this case the image feedback signals are regarded as 0. The experimental result is shown in Fig. 15(c).

Experiments a), b) and c) showed VOR have the ability to cancel the blur of the image on the retinas caused by head movement. However, when the VOR is assumed to be working alone, it would not catch the target accurately, namely, the image feedback control loops are necessary for gazing.

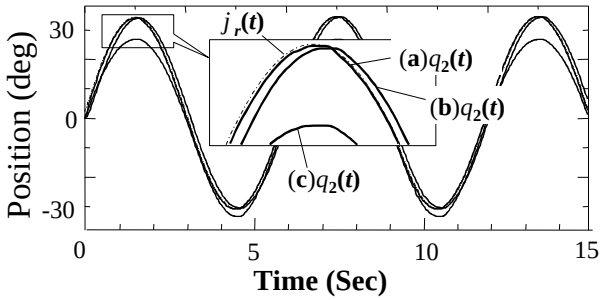

Fig. 15 Response of the binocular axis control system
(a) Fixing target and rotating head,
(b) Fixing head and rotating target,
(c) Rotating head in a dark environment.

VII The Experiments of Head Translations

Since the robot eyes have no degree for translate motion, in the following experiments, the translate signals of head $\dot{x}_h(t)$, $\dot{y}_h(t)$, and image signals from CCD cameras $j_{C\text{-}l}(t)$, $j_{C\text{-}r}(t)$ will be produced by the computers directly.

A. Characteristics of conjugate for head translations

a) Fix the target and translate the head in y_H-axis direction according to the following equation.

$$y_h(t) = 0.5\sin(p\,t/3) \tag{12}$$

So, the input signal of VOR is

$$\dot{y}_h(t) = p/6\cos(p\,t/3) \tag{13}$$

In this case

$$x_h(t) = 0\,\text{m},\quad y_t(t) = 0\,\text{m},\quad x_t(t) = 1\,\text{m},\quad q_0(t) = 0\,\text{rad}.$$

From equations (1) and (2),

$$j_l(t) = -\tan^{-1}\frac{-0.5\sin(pt/3) - r_{he}\sin j_{he}}{1 - r_{he}\cos j_{he}} \tag{14}$$

$$j_r(t) = -\tan^{-1}\frac{-0.5\sin(pt/3) - r_{he}\sin j_{he}}{1 - r_{he}\cos j_{he}} \tag{15}$$

The "retinal slip" signals are calculated as

$$j_{C-l}(t) = j_l(t) - q_1(t) \tag{16}$$

$$j_{C-r}(t) = -j_r(t) - q_2(t) \tag{17}$$

Figure 16(a) is the result of the experiment. Here, only the right eye's rotation $q_2(t)$ is shown.

b) Fix the head and move the target in y_B-axis direction according to the following equation.

$$y_t(t) = -0.5\sin(p\,t/3) \tag{18}$$

In this case

$$x_h(t) = 0\,\text{m},\quad y_h(t) = 0\,\text{m},\quad x_t(t) = 1\,\text{m},\quad q_0(t) = 0\,\text{rad}.$$

From equations (1) and (2),

$$j_l(t) = -\tan^{-1}\frac{-0.5\sin(pt/3) - r_{he}\sin j_{he}}{1 - r_{he}\cos j_{he}} \tag{19}$$

$$j_r(t) = -\tan^{-1}\frac{-0.5\sin(pt/3) - r_{he}\sin j_{he}}{1 - r_{he}\cos j_{he}} \tag{20}$$

The "retinal slip" signals can be obtained. Figure 16(b) is the result of the experiment.

c) Doing the same experiment as a) but in darkness, namely, the "retinal slips" signals $j_{C\text{-}l}(t)$, $j_{C\text{-}r}(t)$ are set as 0. The experiment result is shown in Fig. 16(c).

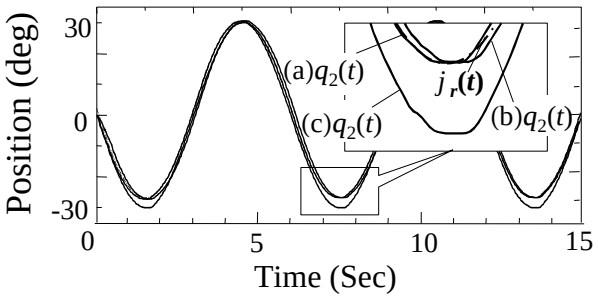

Fig. 16 Response of the binocular axis control system
(a) Fixed target and moving head in y_H-direction,
(b) Fixed head and moving target in y_B-direction,
(c) Moving head in y_H direction in darkness.

B. The characteristics of vergence for translate motions

a) Fix the head and move the target in the x_B-axis direction according to the next equation.

$$x_t(t) = 1 + 0.5\sin(p\,t/3) \tag{21}$$

In this case

$$y_t(t) = 0\,\text{m},\quad x_h(t) = 0\,\text{m},\quad y_h(t) = 0\,\text{m},\quad q_0(t) = 0\,\text{rad}.$$

From equations (1) and (2), the desired values of the robot eyes are obtained:

$$j_l(t) = \tan^{-1}\frac{r_{he}\sin j_{he}}{1 + 0.5\sin(pt/3) - r_{he}\cos j_{he}} \tag{22}$$

$$j_r(t) = -\tan^{-1}\frac{r_{he}\sin j_{he}}{1 + 0.5\sin(pt/3) - r_{he}\cos j_{he}} \tag{23}$$

Using (22) and (23), the retinal slips can be obtained by (16) and (17). Figure 17(a) is the result of the experiment.

b) Fix the target and move the head in the x_h-axis direction according to the following equation.

$$x_h(t) = -0.5\sin(p\,t/3) \tag{24}$$

So, the input signal of VOR is

$$\dot{x}_h(t) = -p/6\cos(p\,t/3) \tag{25}$$

In this case

$$x_t(t) = 1\,\text{m}, \quad y_t(t) = 0\,\text{m}, \quad y_h(t) = 0\,\text{m}, \quad q_0(t) = 0\,\text{rad}.$$

From equations (1) and (2), the desired values of the robot-eyes are the same as (22) and (23). Figure 17(b) is the experimental result.

c) Doing the same experiment as b) but in darkness, i.e. the retinal slips signals $j_{C\text{-}l}(t)$=0, $j_{C\text{-}r}(t)$=0. The experimental result is shown in Fig. 17(c).

Experiments a)~c) showed, similar to conjugate movement, vergence movement also work most effectively when the image feedback and VOR work together.

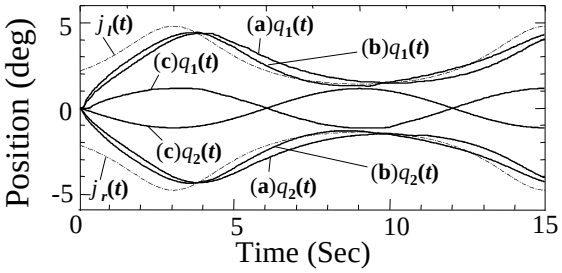

Fig.17 Response of the binocular axis control system
(a) Fixing head and moving target in *x*-direction.
(b) Fixing target and moving head in x direction.
(c) Moving head in x direction in darkness.

VIII Results and Discussions

Many conventional robot eyes are controlled by each eyeball's own control system. Even though the control methods apparently can perform the conjugate and vergence eye movement, some peculiar characteristics of human eyes have never been realized. The solution of fixing the two eyes with each other is out of the question. The skillful relationship of conjugate and vergence eye movements is obtained by the proposed binocular motor control system outlined in this paper.

The characteristic of "same point gazing tendency" was realized using the proposed robot-eye system. The characteristic allows the two eyes to take in a pair of symmetrical images with the same target in the central pits, and we believe this characteristic is one of the necessary conditions for creating a stereovision in the visual cortex using images from both retinas.

When one eye is shut or intercepted by an obstacle, conjugate eye movement causes this eye to follow up the target viewed by the another eye. That means that when the obstacle is removed, the blind eye will find the target viewed by the other eye in an instant.

VOR for both head rotation and head translations is realized using a unified control system, which was shown to work in experiments on the robot-eye system.

Both VOR for head rotation and head translations are realized using a unified control system and the VOR mechanism of the robot-eye system were validated by the experiments.

IV Conclusion

The robot-eyes system with a control system similar to the synthesized binocular motor model based on the physiological characteristics and the anatomical structure of ocular motor system was confirmed to perform several peculiar phenomena of human eyes that conventional robot eyes do not possess. The performances gave us many hints that had never been taken into account before this robot-eyes system was completed, such as "same point gazing tendency," and influences of the centrifugal accelerations of the maculae.

In the near future, more complete oculomotor system models should be built upon the proposed model, and the probable applications in the field of engineering would be of benefit to the development of artificial eyes, which is one of the most important "organs" in robot. Furthermore, the applications in the field of medicine would pioneer some new areas, such as the location diacritics of neuro-ophthalmology using eye movement patterns that correspond to the head or target movement patterns, based on the oculomotor models [16].

References

[1] Deguchi K, Hiura S., "Real-Time Object Tracking and 3D Reconstruction by Active Camera," Transactions of the Society of Instrument and Control Engineers, Vol. 35, No. 5, pp. 675-683, 1999.

[2] Deguchi K, "A Direct Interpretation of Dynamic Image with Camera and Object Motions for Vision Guided Robot Control," International Journal of Computer Vision, Vol. 37, No. 1, pp. 7-20, 2000.

[3] Deguchi K, Hiura S., "3-D Reconstruction by Visual Sensors — Active Visual Sensors for Cooperative Distributed Vision" Journal of the Robotics Society of Japan, Vol. 19, No. 4, pp. 420-426, 2001.

[4] Israeel I., A. Berthoz, "Contribution of the otoliths to the calculation of linear displacement," J. Neuroph., Vol. 62, No. 1, pp. 247-263, 1989.

[5] Matsuyama T, "Cooperative Distributed Vision – Dynamic Integration of Visual Perception, Action, and Communication --," Proc. of Image Understanding Workshop, pp. 365-384, 1998.

[6] Matsuyama T, "Cooperative Distributed Vision Project." Journal of the Robotics Society of Japan, Vol. 19, No. 4, pp. 416-419, 2001.

[7] Matsuyama T, Ukita N, "Cooperative Tracking by Communicating Active Vision Agents." Journal of the Robotics Society of Japan, Vol. 19, No. 4, pp. 439-445, 2001.

[8] Minoh M, Tokai S, "Dynamic Scene Visualization by Multiple Active Cameras," Journal of the Robotics Society of Japan, Vol. 19, No. 4, pp. 446-451, 2001.

[9] Ohmori T, "Binocular Stereo Vision System Using an Eye and Neuron Model.," J Rob Syst, Vol. 3, No. 2, pp. 149 - 163, 1986.

[10] Shibata T, Schaal S, "Fast learning of Biomimetic Oculomotor Control with Nonparametric Regression Networks", Journal of the Robotics Society of Japan, Vol. 19, No. 4, pp. 468-475, 2001.

[11] Wada T, Matsuyama T, "Real-Time Object Tracking with an Active Camera", Journal of the Robotics Society of Japan, Vol. 19, No. 4, pp. 433-438, 2001.

[12] Wada T, Wu X, Tokai S, Matsuyama: "Homography based parallel volume intersection: Toward real-time volume reconstruction using active cameras," Proc. of IEEE Workshop on Computer Architectures for Machine Perceotion (CAMP2000), pp. 331-339, 2000.

[13] Wagner R, Hunter I W, Galiana H L, "A Fast Robotic Eye/Head System: Eye Design and Performance." Proc Annu Int Conf IEEE Eng Med Biol Soc, Vol. 14th, pp. 1584 - 1585, 1992.

[14] Wagner R, Galiana H L, Hunter I W, “A fast robotic eye/head system: control of binocular coordination.” Proc Annu Int Conf IEEE Eng Med Biol Soc, Vol. 16th, pp. 1045 - 1046, 1994.

[15] Wakamatsu H., Kuwano M., and Suda H., "Hardware control system of eye movement by automatic selection of control laws using neural networks”, *Trans.IEE Japan*, **114-C**, pp. 1024-1030, 1994.

[16] Zhang X., H. Wakamatsu: A mathematical model for binocular vestibular-ocular reflex and its application on topographic diagnosis. Japanese Journal of Applied Physiology, Vol.**29, No.**2, pp.123-131, 1999.

[17] Zhang X., H. Wakamatsu, “A mathematical model for binocular motor system based on neural network in brain stem,” IEEE Trans Biomed Eng,, Vol.****, No.***, pp.***-***, 2002.

[18] http://www.tmd.ac.jp/med/mtec/wakamatsu/research/movies.htm